Anti-freezing conductive zwitterionic composite hydrogels for stable multifunctional sensors

Zhang, Zeyu; Raffa, Patrizio

IMPORTANT NOTE: You are advised to consult the publisher's version (publisher's PDF) if you wish to cite from it. Please check the document version below.

Document Version
Publisher's PDF, also known as Version of record

[Link to publication in University of Groningen/UMCG research database](#)

Anti-freezing conductive zwitterionic composite hydrogels for stable multifunctional sensors

Zeyu Zhang, Patrizio Raffa [*]

Smart and Sustainable Polymeric Products, Engineering and Technology Institute Groningen (ENTEG), Faculty of Science and Engineering, University of Groningen, Nijenborgh 4, 9747 AG Groningen, The Netherlands

ABSTRACT

Zwitterionic conductive hydrogels have shown potential application in wearable strain and pressure sensors. However, there are still fundamental challenges to achieve zwitterionic hydrogels with excellent mechanical properties, able to keep flexibility at sub-zero temperatures. To overcome these limitations, a zwitterionic conductive hydrogel was fabricated in this work by in-situ polymerization of aniline (ANI) monomer in a copolymer of sulfobetaine methacrylate (SBMA) and acrylic acid (AA) matrix. The obtained hydrogel possesses outstanding anti-freezing performance (without obvious loss of stretchability at −18 °C) and water-retaining properties, due to the introduction of LiCl on the zwitterionic polymer matrix. The synergy of chemical and physical crosslinking between poly (SBMA-co-AA) and polyaniline (PANI) networks enhance the mechanical performance of the zwitterionic hydrogel, that exhibits a fracture tensile strength of 470 kPa, and a fracture strain up to 600 %. Additionally, the integration of PANI confers stable conductivity (2.23 S m^{-1}, maintained at 1.89 S m^{-1} even at −18 °C), high sensitivity (GF = 1.74), and short response and recovery times (223 ms and 191 ms, respectively). The hydrogel can be applied as a flexible sensor to accurately detect various human motions. This work provides a feasible strategy for developing wearable multifunctional sensors in a wide working temperature range.

1. Introduction

In recent years, tremendous efforts have been devoted to developing soft electronic materials to address the growing global demand for flexible electronics, aimed at improving healthcare monitoring and human–machine interactions [1–4]. Flexible electronics exhibit a range of desirable characteristics, including high conductivity, non-flammability, thermal, chemical, and electrochemical stability, as well as remarkable flexibility and mechanical properties [5–7]. Conductive hydrogels (CHs) have emerged as promising materials for flexible electronics due to their biological tissue-like texture, high water content, high flexibility and stable conductivity [8–10]. CHs are typically based on composite materials constituted by a cross-linked hydrophilic polymer matrix and a conductive filler, including carbon materials [11], ionic liquids [12], conductive polymers [13] and metallic nanoparticles [14]. In particular, the conductive polymers that can be incorporated into hydrogels matrix, not only improve the electrical conductivity, but also enhance their mechanical properties.

Polyaniline (PANI), an intrinsically conductive polymer, has been used for the fabrication of conductive hydrogels due to its notable electrical conductivity and cost-effectiveness [15,16]. However, the inherent delocalized π-electron system along the conjugated polymer backbone of polyaniline results in rigidity of the polymer chains. This rigidity can lead to challenges like inadequate dispersion within the hydrogel matrix and a propensity to form distinct domains of aggregated chains. Consequently, these factors can weaken the overall network integrity and result in suboptimal mechanical properties. Wang et al. [17] prepared a conducting hydrogel through the in-situ polymerization of PANI combined with an aramid nanofiber–polyvinyl alcohol (ANF–PVA) hydrogel as a template. The sensor exhibited favorable conductivity, toughness, stability, and sensitivity; however, the tensile strain of the hydrogel was limited to 140 %. Similarly, Jiao et al. [18] developed a cellulose nanofibrils/polyacrylic acid (PAA)/PANI hydrogel via an in-situ polymerization method involving both physical and chemical cross-linking, where PANI was chemically doped and ionically crosslinked with phytic acid (PA). Although the hydrogel's tensile strain was improved, its tensile strength only reached a maximum of 74.98 kPa. Achieving both high flexibility and good stretchability remains a

significant challenge in the design of such materials.

A general problem encountered with hydrogels is their poor freezing tolerance. Due to high water content, they become rigid and fragile at sub-zero temperatures, due to ice crystals formation, severely limiting their practical applications at low temperatures. To address this issue, anti-freezing agents such as glycerol and ethylene glycol [19,20], as well as salts like lithium chloride and sodium chloride [21–23], have been incorporated into hydrogels to lower the freezing point of water. While polyols are known to grant anti-freezing properties to hydrogels, they have been found to have a negative impact on their conductivity [24]. By contrast, incorporating inorganic electrolytes into CHs has been shown to enhance both the conductivity and anti-freezing properties of the resulting hydrogels [25]. Despite the potential of these hydrogels for use in low-temperature sensors, it remains challenging to find a proper balance between anti-freezing properties, sensitivity, and mechanical properties required for motion sensor applications.

Zwitterionic monomers, also known as internal salts, are small molecules containing cations and anions on the same unit, which can be applied as biocompatible materials due to their ultralow fouling properties and excellent biocompatibility [26–28]. The positive and negative ions of polyzwitterions can be separated under the action an external electric field, providing ionic conductivity [29]. Zwitterionic polymers can be used as a potential hydrogel matrixes for highly conductive wearable or implantable devices [30,31]. In addition, the introduction of salts into zwitterionic polymer hydrogels further improves their anti-freezing properties. The electrostatic interaction between the zwitterion and the salt ion may contribute to the conductivity via ions hopping mechanisms [32,33]. However, hydrogels based on zwitterionic polymers are typically rather weak, due to their superhydrophilic characteristics [34,35]. By combining zwitterions with other polymers, the toughness or stretchability of zwitterionic hydrogels can be improved to a certain extent. Xu et al. [36] reported a zwitterionic copolymer-based hydrogel by polymerization of acrylic acid (AA), octadecyl methacrylate and sulfobetaine methacrylate (SBMA). The stress at break of the hydrogel is enhanced to ~140 kPa, yet the elongation at break is only 175 %. Sui et al. [37] developed a poly (sulfobetaine-co-acrylic acid) hydrogel with anti-freezing properties and self-regeneration abilities in the presence of LiCl salt. Although the elongation at break of the hydrogel is improved to ~800 %, the toughness of the hydrogel is still not very high (breaking stress ~60 kPa). Hence, there is a pressing need to identify a viable approach to create intelligent conductive hydrogels that exhibit remarkable strain capacity, exceptional toughness, and effective anti-freezing properties.

In this work, building on the mentioned previous literature work, we fabricated a zwitterionic hydrogel with anti-freezing property by copolymerizing SBMA and AA in the presence of LiCl salt, with improved characteristics. Due to the inhibitory effect of LiCl on water crystallization, the composite hydrogel is still able to withstand large deformations after being stored at $-18\,°C$ for up to 30 days. To improve the mechanical performance and conductivity of the hydrogel, we introduced the conducting PANI hydrogel network into the poly (SBMA-co-AA) hydrogel matrix by an in-situ polymerization method. The electrostatic interaction and intermolecular hydrogen bonding among sulfonate, amino, hydroxyl and aniline groups endow the hydrogel with excellent tensile and compressive properties, superior to those of previously reported analogous materials. In addition, the interconnected PANI network imparts the hydrogel high conductivity, which exhibits fast response and measurement accuracy for strain and pressure sensing. Lastly, the wearable sensor formed from poly (SBMA-co-AA)/LiCl/PANI (PSA/LiCl/PANI) hydrogel can detect various human motions, demonstrating its great potential in wearable electronics. This combination of a zwitterionic hydrogel, LiCl and PANI conductive filler, has not been reported in literature to the best of our knowledge, in the preparation of strain and pressure sensors operating at low temperatures.

2. Experimental sections

2.1. Materials

N-(3-sulfopropyl)-N-(methacryloxyethyl)-N,N-dimethylammonium betaine (SBMA, 99 %), Acrylic acid (AA), Aniline (ANI, ≥99.5 %), phytic acid (PA, 50 wt % in water), ammonium persulfate (APS, 98 %), N,N′-methylenebisacrylamide (MBAA, 98 %) and LiCl were purchased from Sigma-Aldrich. Milli-Q water was used throughout the experiments.

2.2. Synthesis of conductive PSA/LiCl/PANI hydrogels

Composite hydrogels were made in two steps. PSA/LiCl hydrogels were first synthesized via free radical polymerization: monomers (SBMA and AA), LiCl, cross-linker (MBAA), and initiator (APS) were dissolved in Milli-Q water, sonicated, and polymerized at 60 °C for 6 h in a mold with glass plates and a 3 mm-thick silicone rubber spacer. Detailed parameters are shown in Table S1. PSA/LiCl hydrogels were allowed to reach a constant weight at room temperature, followed by immersion for 12 h in ANI/PA/APS solutions of varying concentrations, pre-cooled at 4 °C, leading to conductive PSA/LiCl/PANI hydrogels formation.

2.3. Characterization

Attenuated total reflection infrared (ATR-FTIR) spectra in the wavenumber range 500–4000 cm^{-1} were collected by IRTracer-100 (SHIMADZU) with 32 scans at a resolution of 4 cm^{-1}. Elemental analysis was performed with a Euro Vector EA3000 CHNS from ELMENTAR. The surface morphology and surface chemistries of the samples were evaluated with a scanning electron microscope (SEM) and energy-dispersive X-ray spectroscopy (EDX) with Nova NanoSEM 650. The samples were freeze-dried for 72 h and then fractured in liquid nitrogen and coated with a thin layer of gold before taking SEM images. The mechanical properties of the composite hydrogels were measured by a universal testing machine (Tinius Olsen H25KT) equipped with a 1 kN load cell. They were cut into dumbbell-shaped of 20 mm × 5 mm × 3 mm for tensile testing at a speed of 50 mm min^{-1}. The samples with a diameter of 12 mm and a height of 20 mm were used for compressive testing at 50 mm min^{-1}. For mechanical properties at lower temperatures, the hydrogel was stored in a refrigerator for several days before being promptly subjected to rapid testing (1000 mm/min). Dynamic mechanical analysis (DMA 8000, PerkinElmer) was employed to conduct rheological tests on the hydrogels over a temperature range of $-40\,°C$ to 25 °C with a heating rate of 2 °C·min^{-1}. The storage moduli (G′) of the hydrogel were determined by measuring the response at a frequency sweep (ω) of 10 rad s^{-1} and a constant strain (γ) of 1 %.The freezing points of the hydrogels with different concentrations of LiCl were investigated by differential scanning calorimetry (TA Instruments, DSC Q2000) with a cooling system (TA Instruments, RCS90). In the cool-warm process testing, the samples were cooled from 25 to $-70\,°C$ at a rate of 5 °C min^{-1} and the warm up to 25 °C after equilibrating at $-70\,°C$ for 5 min. Rheological tests were performed by TA instrument (Discovery HR-2) with an 8 mm parallel plate. The storage and loss moduli (G′ and G″) of the hydrogels at 0.1–100 % strain was measured at a constant angular frequency of 1 Hz. The values of G′ and G″ in the frequency range 0.1–100 rad s^{-1} were measured at room temperature with a fixed strain of 1 %. The swelling ability of a hydrogel was quantified by the swelling ratio, which was calculated as the change in mass from the dried sample (M_0) to the swollen hydrogel at time t (M_t), divided by the mass of the dried sample (M_0). This can be represented mathematically as ($M_t - M_0$)/M_0.

2.4. Electrical measurements

The resistance of hydrogels was evaluated by a digital multimeter (Velleman DVM855). The electrical conductivity δ was determined ac-

cording to the following equation:

$$\delta = \frac{L}{R \times S} \quad (1)$$

Where the L is the length (cm), R represents the resistance of hydrogel (Ω), and S is the cross-section area of the hydrogel (cm^2). To prepare a strain sensor, the hydrogel was cut into a parallelepiped shape of 20 mm $\times$ 5 mm $\times$ 3 mm, and two individual copper wires were attached to both ends of the strip through copper tape. The dynamic electrical response signals were simultaneously recorded by a digital multimeter (Keysight U2741A) during the stretching of the strain sensors in the tensile machine. The conductive signals of hydrogel under different strains were represented by the relative resistance change (($R - R_o$)/R_o), where R and R_o are the resistances of the hydrogel in the original and real-time states, respectively. The sensitivity of strain sensor (gauge factor (GF)) was characterized by the following equation:

$$GF = \frac{(R - R_o)/R_o}{\varepsilon} = \frac{\Delta R/R_o}{\varepsilon} \quad (2)$$

where ε is the strain of the hydrogel under tensile strain. For the pressure sensor, the hydrogels were cut into a shape of 5 mm $\times$ 5 mm $\times$ 3 mm and a 4 $\times$ 4 array connected by copper tape was constructed. The variational resistance was recorded using a Keysight U2741A digital multimeter and a software "Keysight BenchVue" in a laptop. Hydrogels were adhered to different parts of human body with tape and connected to digital multimeter with copper wires to monitor human movements.

3. Results and discussion

3.1. Fabrication strategy of PSA/LiCl/PANI hydrogel

The PSA/LiCl/PANI hydrogels were synthesized via a facile two-step process, as described in the experimental section, and illustrated in Fig. 1a. Within this zwitterionic hydrogel system, anions and cations present on SBMA chains can interact by electrostatic forces with Li$^+$ and Cl$^-$ ions. Hydrogen bonds and electrostatic interactions formed between COOH groups from AA and zwitterions serve as physical cross-linking points, further strengthening the hydrogel. The introduction of the rigid and conductive PANI chains in the PSA/LiCl matrix, was aimed at improving both mechanical and conductive properties. Variable amounts of PANI were introduced, by using ANI solutions at different monomer concentration in the second step (Fig. 1). The resulting hydrogels were denoted PSA/LiClx/PANIy, where $\times$ represents LiCl concentration (M), and y refers to ANI concentration in the PANI precursor solution (mol L^{-1}). The composition of all prepared hydrogels is reported in Table S1.

PA molecules act as cross-linking points for PANI polymer chains via interactions with the —NH groups, forming a three-dimensional network, which interpenetrates with the hydrogel one. After the ANI was successfully polymerized, the color of the hydrogel changed from transparent to dark, indicating formation of the PANI network (Fig. 1b (i)). Elemental analysis (Table S2), provides evidence of the incorporation of PANI, as reflected in the increase in the overall nitrogen content
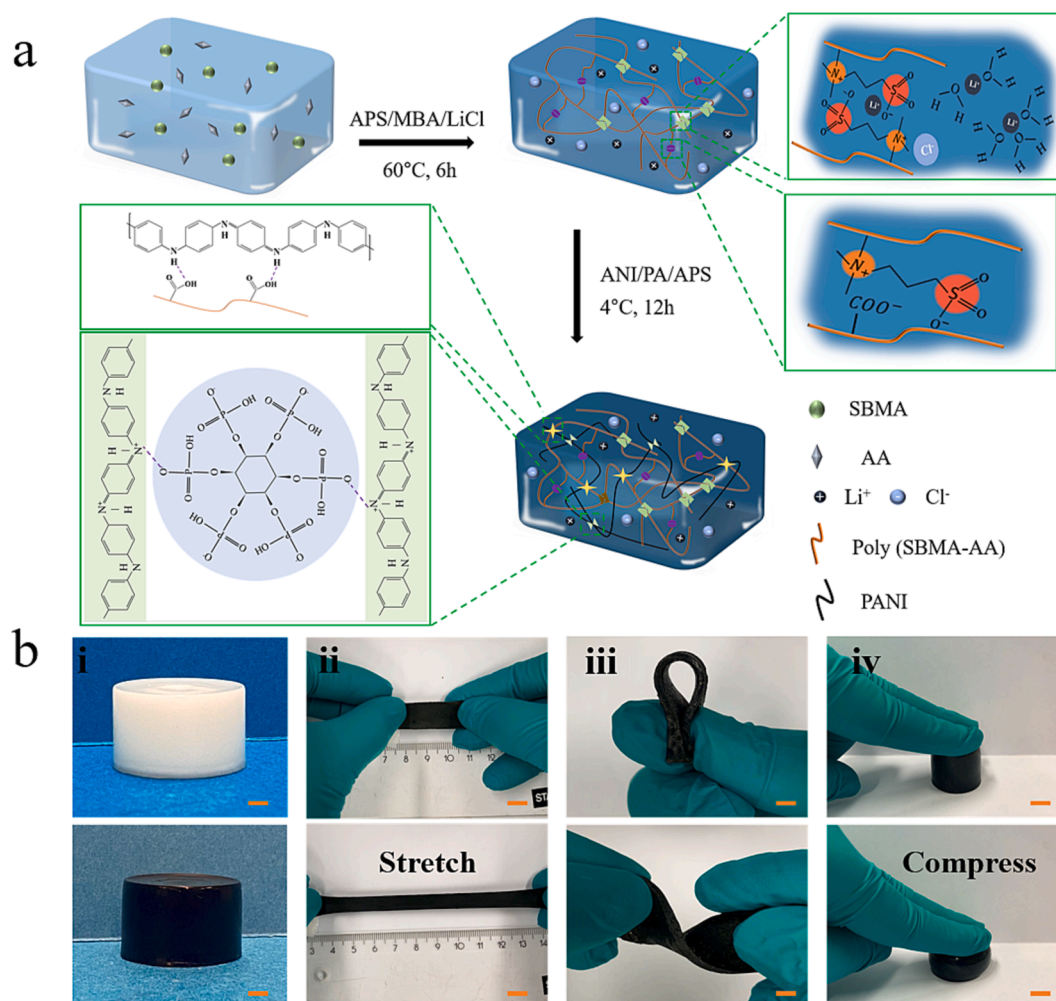

Fig. 1. (a) Schematic diagram of the preparation process of the PSA/LiCl/PANI hydrogel and its network structure. (b) Photographs of the PSA/LiCl and PSA/LiCl/PANI hydrogel (i), and Photographs showing the PSA/LiCl$_2$/PANI$_{0.30}$ hydrogel was stretched (ii), bended and twisted (iii), and compressed (iv). Scale bar: 1 cm.

after introduction of the latter.

The obtained zwitterionic hydrogels could be stretched, bent, curled, or compressed, and return to their original shape after the release of external forces (Fig. 1b (ii–iv)). The chemical structure of PSA/LiCl/PANI hydrogel was also analyzed using ATR-FTIR spectroscopy (Fig. S1). The N—H and C—C stretching vibrations of the quinoid and benzenoid rings in PANI were identified by the absorption peaks observed at 3349 cm^{-1}, 1633 cm^{-1}, and 1496 cm^{-1}. The peaks observed at 1168 cm^{-1} and 1060 cm^{-1} are attributed to combination of in-plane C—N and C—H bending vibrations [38,39]. Characteristic peaks of both PSA/LiCl and PANI could be observed in the PSA/LiCl/PANI hydrogel, accompanied by a peak shift. For instance, the bands of N—H showed a blue shift to 3236 cm^{-1}, indicating hydrogen bond interactions between in the PSA and PANI; the peak at 1496 cm^{-1} in PANI, shifted to 1458 cm^{-1}, and the peak at 1177 cm^{-1} and 1249 cm^{-1} in the PSA/LiCl matrix, shifted to 1247 cm^{-1} and 1296 cm^{-1} respectively [40]. The obtained results suggest that there are interactions occurring between the PSA and PANI networks, causing peaks shifts. The presence of Li, Cl and P element in PSA/LiCl$_2$/PANI$_{0.30}$ can be evidenced by the EDX mapping, further demonstrating the successful synthesis of the composite hydrogel (Fig. S2).

In a first screening, tensile properties of PSA/LiCl/PANI hydrogels at fixed amount of PANI and LiCl, but with different SBMA/AA ratios were investigated. The elongation decreases with increasing SBMA/AA ratio, because hydrogels with higher AA content exhibit stronger polymer chain intermolecular interactions (Fig. S3) [37,41]. Therefore, a SBMA/AA mass ratio of 1:2 was selected for further studies. The influence of LiCl and PANI concentration on mechanical and rheological properties was systematically investigated. The fracture strain of the PSA/PANI$_{0.30}$ hydrogel reached 698 % in the absence of LiCl. Gradual incorporation of LiCl led to a decrease in this value, reaching 492 % at a salt concentration of 3 M (Fig. 2a), still a good value for sensing applications. LiCl can weaken hydrogen bond and screen electrostatic attraction between opposite sign charges in the hydrogel structure, reducing the effective crosslinking density of the polymer network [21,32,42]. Finally, it has been confirmed that mechanical properties of hydrogels could be effectively improved by the introduction of PANI [43,44]. As exhibited in Fig. 2b, both tensile strength and elongation at break of the composite hydrogels increased simultaneously when the PANI concentration was increased from 0 up to 0.30 M. The elongation at break reached a maximum at 602 % at a 0.30 M concentration of ANI. These properties surpasses those obtained with analogous hydrogels from previous work [32,34,36,45]. By further increasing the content of PANI to 0.60 M, the elongation at break slightly dropped to 480 %, even though the tensile strength keeps increasing to a maximum of 557 kPa. The toughness of the hydrogel also slightly decreased to 1424.77 ± 21.55 kJ m^{-3} (Fig. S4). The reason for this result is that excess ANI can accumulate in the matrix causing stress concentration, while the compact PANI network can also affect the migration of poly (SBMA-AA) chain [8,18,46].

The strong interpenetration between the PANI and poly (SBMA-AA) networks can be inferred from the SEM images (Fig. 3a to 3e), that show a more compact structure, indicative of increased cross-linking density, as the PANI amount increases; this is beneficial for the mechanical strength [44,47]. The PSA/LiCl hydrogels have larger pore size and see-through hole structure (Fig. 3a), indicating that its network is relatively loose. As the ANI concentration increased from 0.15 to 0.45 M, the pore size of the PSA/LiCl/PANI hydrogels decreased, to finally turn into a closed-pore structure at 0.6 M PANI. The results confirm that the introduction of PANI facilitate the establishment of composite hydrogels with compact structure and higher cross-linking density. This is also demonstrated by the lower equilibrium swelling ratio of PSA/LiCl/PANI hydrogels than pure PSA/LiCl hydrogels (Fig. 3f). The mechanical stability of the PSA/LiCl/PANI hydrogels was further studied through loading–unloading tests (Fig. S5a, b). The observed hysteresis loops during stretching cycles (with a hysteresis value of 9.46 kJ m^{-3} after 20 cycles of stretching) were a result of the partial breaking of the abundant non-covalent interactions in the hydrogel, including hydrogen bonds and electrostatic interactions, during the stretching process [48]. After 20 cycles of loading–unloading tests at strain of 100 %, the stress value was 100.60 kPa, not significantly lower than the first stretch cycle (104.25 kPa). These results suggest that non-covalent bonds can effectively dissipate part of the energy and reconstruct the network structure, enabling the hydrogel to achieve good durability and compliance [45,49].

The rheological behavior of the hydrogels was also studied. It is well-known that the storage modulus (G′) reflects the energy stored elastically in the gel structure during applied stress, while the loss modulus (G″) reflects the energy dissipated by viscous response. As shown in Fig. 4a, the G′ of PSA/LiCl/PANI hydrogels exceeded its G″ values in a large range of strain at constant angular frequency (γ = 0.1–100 %, ω=1.0 Hz), confirming that their networks are in an elastic gel state rather than in a viscous sol state. The G′ value increases gradually with the concentration of ANI, demonstrating that PANI enhances mechanical properties of the composite hydrogels. This is mainly due to the fact that PANI is rigid, but it also provides more physical cross-linking points, via hydrogen bonds and electrostatic interactions with the poly (SBMA-AA) chains. Within the frequency range ω = 0.1–100 rad s^{-1}, the value of G′ of increased with increasing the angular frequency, revealing a slightly frequency-dependent viscoelastic modulus (Fig. 4b). Through dynamic step-strain rheology, the excellent strain recovery performance of the hydrogel was demonstrated (Fig. 4c). At a small shear strain of 1 % for 100 s, the G′ of the hydrogel was always higher than G″, indicating a solid-like elastic network. The G′ value dropped to 5 kPa when the hydrogel was subjected to a large shear strain of 200 %. When the shear strain returned to 1 %, the G′ value recover to original state immediately
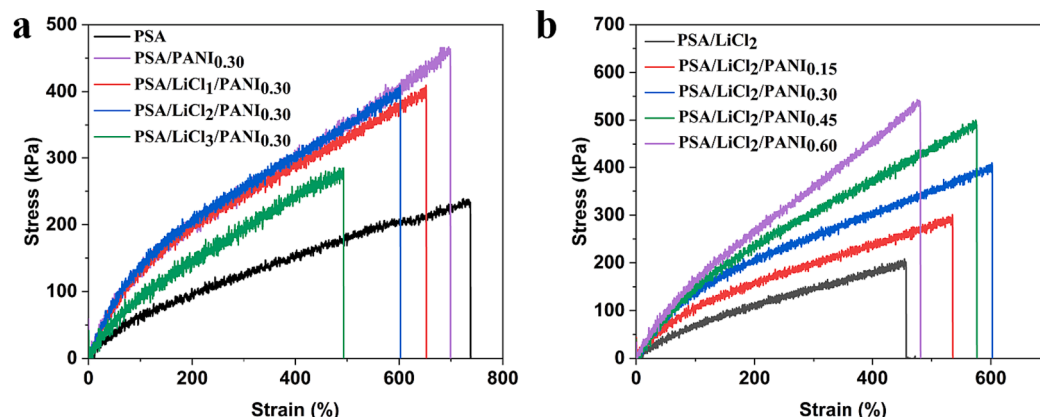

Fig. 2. Tensile stress–strain curves of hydrogels (a) with different LiCl concentrations. (b) With different ANI concentrations.
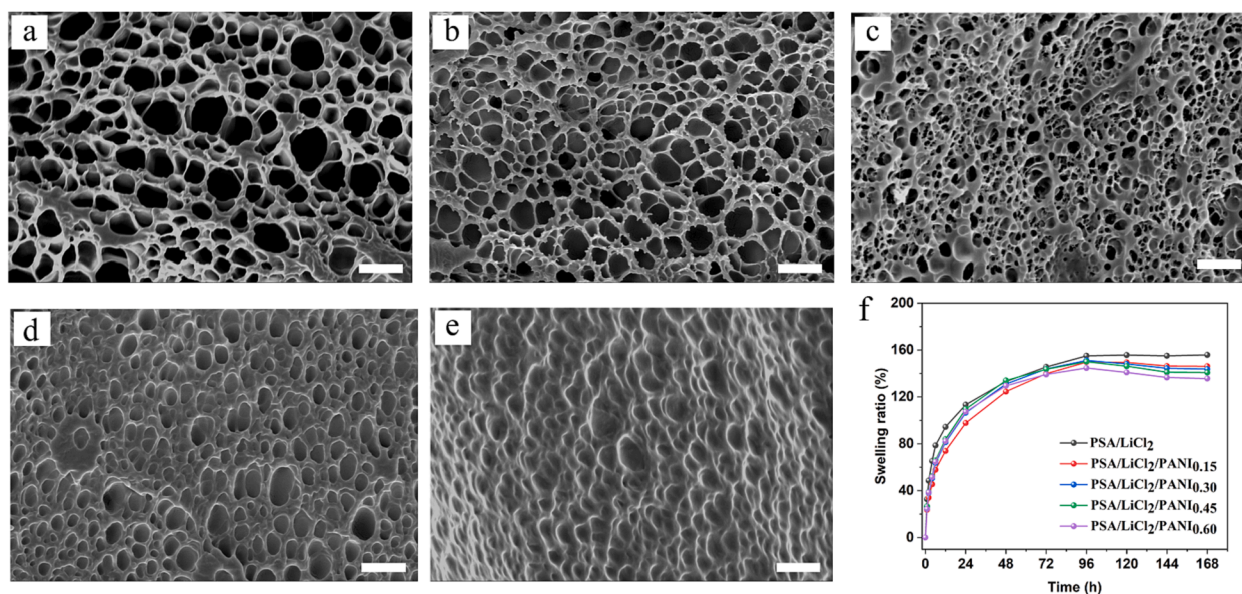
Fig. 3. SEM images of (a) PSA/LiCl$_2$ hydrogel and PSA/LiCl$_2$/PANI$_y$ hydrogels with different PANI concentrations: (b) 0.15 M, (c) 0.30 M (d) 0.45 M, (e) 0.60 M. (f) Swelling ratio of hydrogels with different PANI concentrations from 0.15 to 0.60 M. Scale bar: 50 μm.
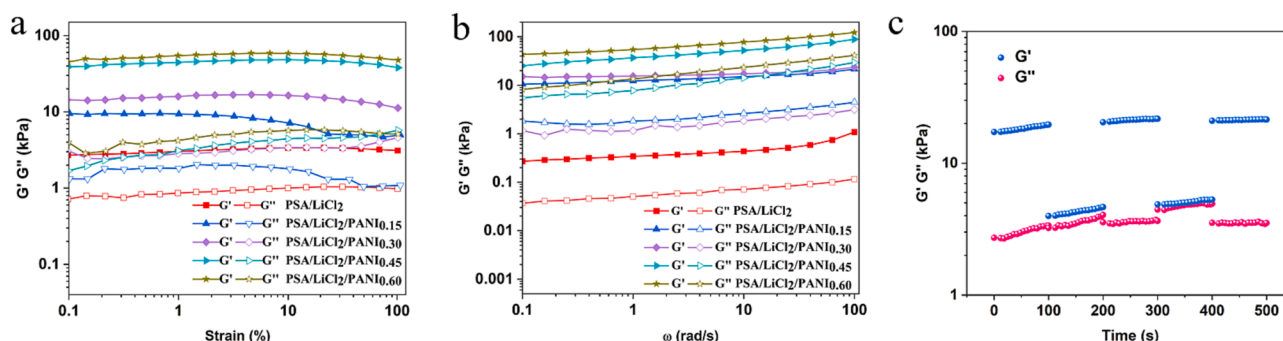

Fig. 4. Dynamic viscoelasticity of hydrogels with different ANI concentrations at 25 °C: (a) variation of G′ and G″ with strain (at fixed ω = 1.0 Hz), (b) variation of G′ and G″ with frequency from 0.1 to 100 rad s^{-1}; (c) dynamic stepwise strain amplitude tests of PSA/LiCl$_2$/PANI$_{0.30}$ hydrogel.

and maintained a similar value for 100 s.

3.2. Anti-freezing properties and water retention of PSA/LiCl/PANI hydrogels

Due to the large amounts of water, traditional conductive hydrogels freeze and become rigid at subzero temperatures, losing stretchability. Here, due to the incorporation of lithium chloride, the solidification of water can be effectively reduced. Fig. 5a (i) shows that the hydrogel without LiCl can be frozen into a hard solid after being placed at −18 °C for 30 days and could be easily broken upon bending. When LiCl is added as an antifreeze agent, the resulting PSA/LiCl/PANI hydrogels can still be bent, twisted and stretched after being stored at −18 °C for 30 days (Fig. 5a (ii–iv), as shown in Supporting Movie 1 (this movie was shot immediately after taking the hydrogel out of the freezer; the surface temperature of the hydrogel is shown in Fig. S6). The tensile strength of the hydrogel increases, while the maximum strain decreases with the reduction in environmental temperature from room temperature to −10 °C, still keeping a very good stretchability, up to more than 400 %. This intriguing behavior can be attributed to the reinforcement of noncovalent interactions at lower temperatures (Fig. S7a) [48]. Similarly, the hydrogel still could be compressed at −10 °C without fracture (Fig. S7b). This further demonstrates the applicability of the hydrogel at subzero temperature. As depicted in Fig. 5b The PSA/PANI hydrogel

displayed a notable increase in G′, which could be due to water crystallization occurring during the cooling process. In contrast, when LiCl was introduced into hydrogel, the effect becomes much less pronounced and the onset was shifted to lower temperature. The PSA/LiCl$_3$PANI$_{0.30}$ hydrogel displayed negligible changes in G′ over the temperature range from −40 °C to 25 °C, suggesting stable mechanical properties. The DSC curve shown in Fig. 5c, further confirm the effect of LiCl on the low-temperature behavior. The freezing point of all PSA/LiCl/PANI hydrogels was in fact much lower than that of hydrogel without LiCl. A large exothermic peak located at −19.5 °C can be observed in the PSA/PANI hydrogel, while the exothermic peak shifted to −28.2 °C when the LiCl concentration increased to 1 M. The freezing peak completely disappeared at a LiCl concentration of 2 M, demonstrating that the composite hydrogels did not form ice in the entire interval from −70 °C to 25 °C. Moreover, the PSA/LiCl/PANI hydrogels showed much better water retention than the PSA/PANI hydrogel (Fig. 5d). When placed in the open at room temperature for 14 days, the PSA/PANI hydrogel only retained 45 % of its initial mass. Increasing amounts of LiCl were associated with higher water retention (Fig. 5e). This can be explained by the strong hydration of the Li$^+$ ion: more energy is required to overcome the electrostatic interactions and remove water molecules from the system. Considering the combination of excellent mechanical performance and anti-freezing property, the hydrogel prepared with 2 M LiCl and 0.30 M ANI was selected for sensing tests.
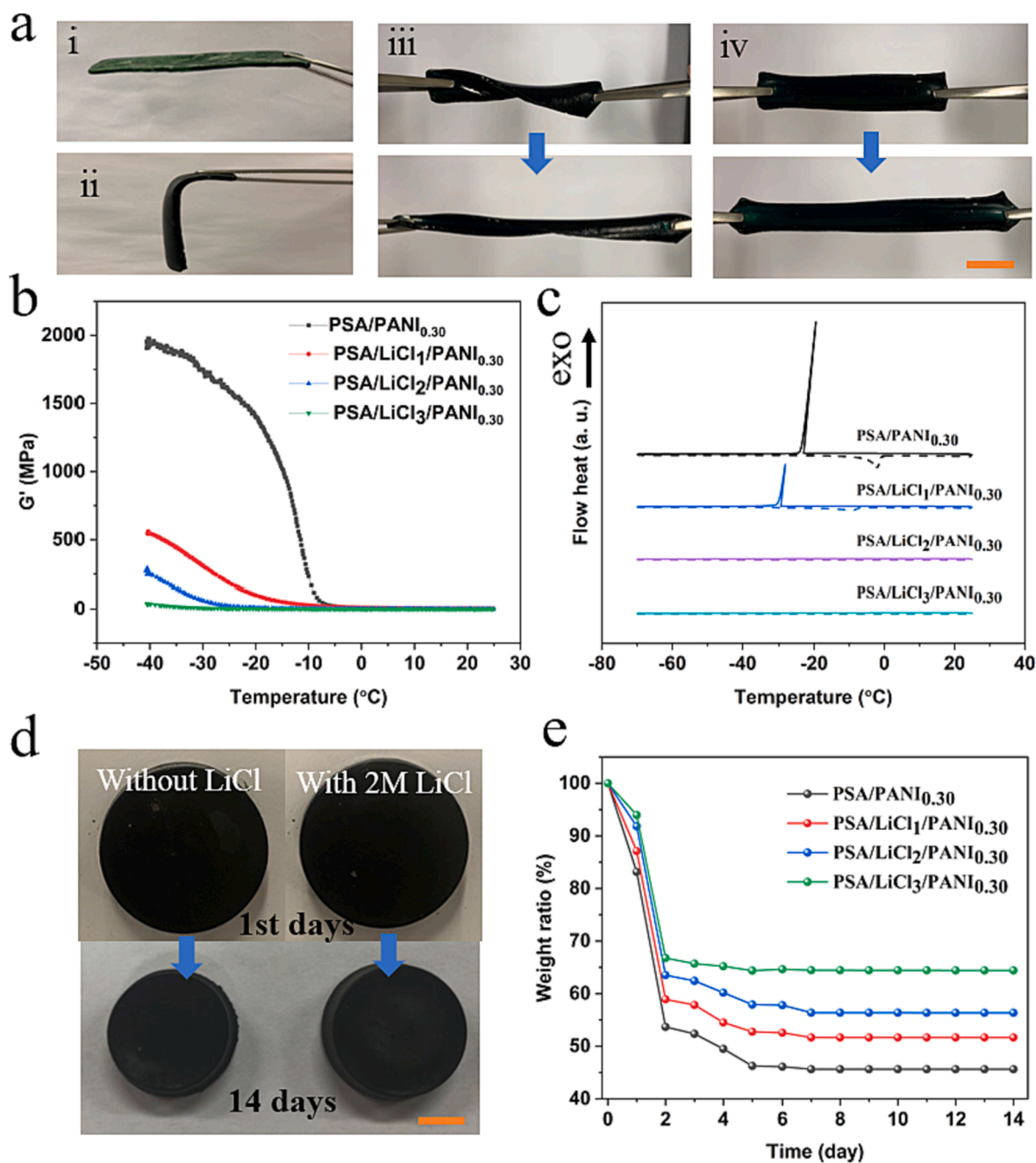
Fig. 5. (a) Photographs of the PSA/PANI hydrogel at −18 °C (i); the PSA/LiCl/PANI hydrogel at −18 °C (ii); twisting (iii) and stretching (iv). (b) Storage modulus of hydrogels from 25 °C to 40 °C. (c) DSC curves of hydrogels with different concentration of LiCl. (d) Photographs of the PSA/PANI hydrogel (left) and the PSA/LiCl$_2$/PANI$_{0.30}$ hydrogel (right) on the 1st and 14th days in open air. (e) Evolution of water loss with time in hydrogels with different concentration of LiCl (stored in a chamber at 22 °C and 53 % relative humidity). Scale bar: 1 cm.

3.3. Application of PSA/LiCl$_2$/PANI$_{0.30}$ hydrogels as flexible sensors

The conductivity of the prepared PSA/LiCl/PANI hydrogels increased with increasing PANI concentration, reaching values up to 2.23 S m^{-1} when 0.60 M ANI was used (Fig. S8); this is due to the formation of a more continuous conductive networks in the hydrogel. Even at −18 °C, the hydrogel still possessed good conductivity (1.89 S m^{-1}), exceeding that achieved in some previous work [50–52]. As shown in Fig. S9, when the hydrogel was connected to a circuit with a small light emitting diode (LED), a brightness change could be observed when the hydrogel was stretched or compressed (both at room temperature and at −10 °C), demonstrating that the geometrical change causes the change of the conduction path [53]. Due to their excellent mechanical

properties and high conductivity, PSA/LiCl/PANI hydrogels were considered as ideal candidates for flexible sensors. The electromechanical performance of the composite hydrogels was evaluated by relative resistance change $\Delta R/R_o$, as a function of applied strain. When the hydrogel was stretched, the resistance increased (Supporting movie 2). Fig. 6a shows the strain sensory performance. As shown in Fig. 6b, the response signals of the PSA/LiCl$_2$/PANI$_{0.30}$ hydrogels at small strains (5 %, 10 %, 20 % and 50 %) were significantly different in five cycles of the stretch-release process, and could generate targeted feedback electrical signals in real-time. The signals were more pronounced as the strain increased. Similarly, the hydrogel could also output different stable signals under large deformations (100 %, 200 %, 300 % and 400 %, Fig. 6c), and the patterns of each cycle of the same deformation were
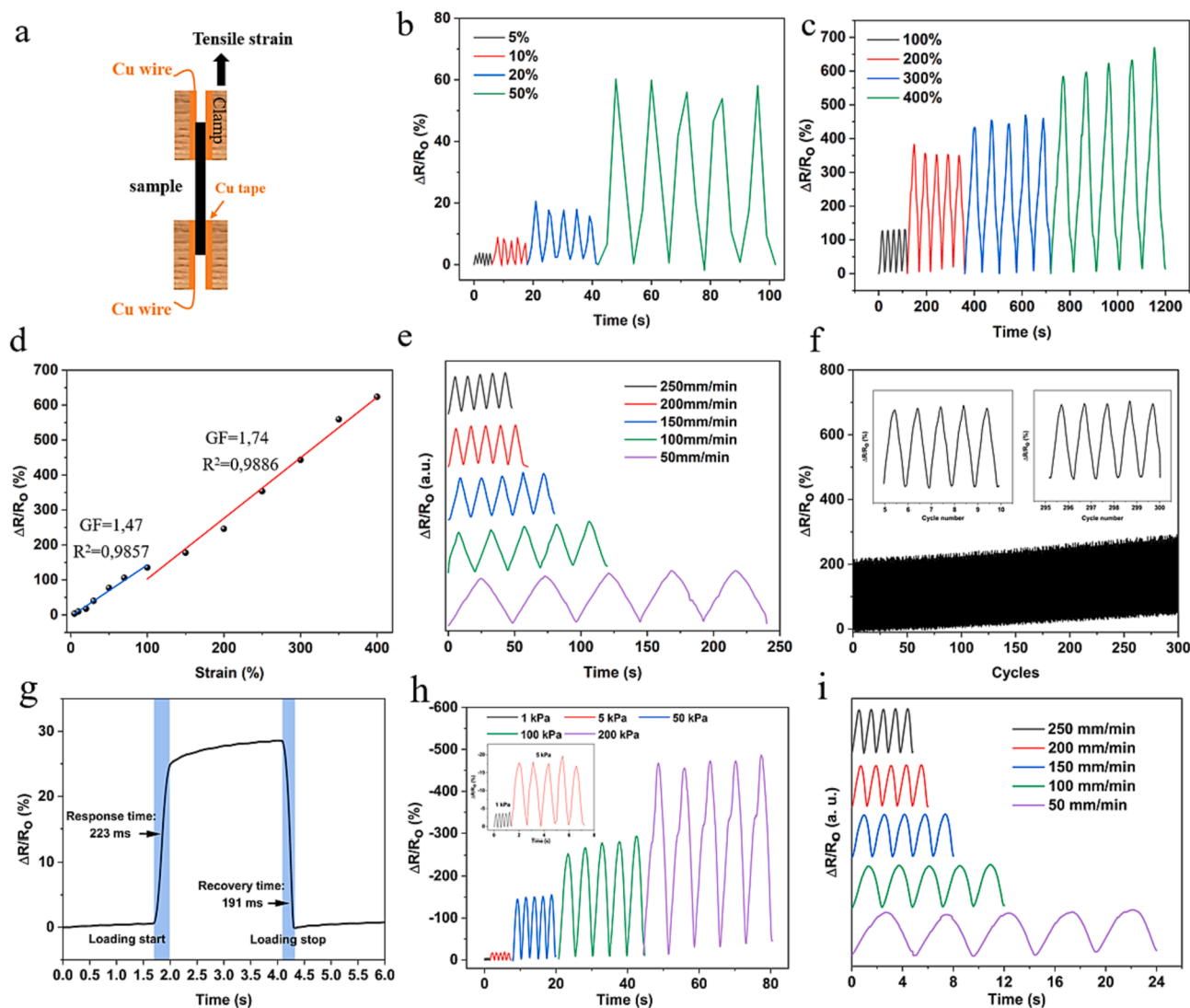
Fig. 6. (a) Schematic illustrations of the methods applied for the tensile sensory performance tests. Relative resistance variation of the sensor for a strain (b) 5–50 %. (c) 100–400 %. (d) Response curves of the sensors. (e) Relative resistance changes of sensor under cyclic loading–unloading with a strain of 100 % at different tensile rates (from 50 to 250 mm min^{-1}). (f) Relative resistance changes of sensor under a cyclic test of 100 % tensile strain for 300 cycles. (g) Response time and recovery time of a hydrogel strain sensor. (h) Relative resistance variation of the sensor for a pressure 1–200 kPa. (i) Relative resistance changes of sensor under cyclic loading–unloading with a pressure of 50 kPa at different tensile rates (from 50 to 250 mm min^{-1}).

highly similar. Under a stepwise strain change, a stepwise signal pattern was obtained, indicating that the PSA/LiCl$_2$/PANI$_{0.30}$ hydrogels can detect and distinguish different levels of deformation with excellent reliability.

Sensitivity and responsivity are two important properties of hydrogel-based sensors. The sensitivity of PSA/LiCl$_2$/PANI$_{0.30}$ hydrogel-based sensor was evaluated using the gauge factor (GF). The higher the value of GF, the better the sensitivity of hydrogel based sensor. In this case, the GF values was 1.47 in the 0–100 % strain range, and further increased to 1.74 in the 100–400 % strain ranges (Fig. 6d). The lower detection threshold was observed at 0.3 % strain, with a corresponding GF of 1.33 within the strain range of 0.3 % to 4 % (Fig. S10). As shown in Fig. 6e, the flexible sensor based on hydrogels could respond accurately under cyclic loading–unloading processes at diverse strain rates. It can be clearly seen that the response signals for displacement rates from 50 to 250 mm min^{-1} are almost identical, and the resistance signals caused by stretching and releasing show a rather rapid rise and fall within one cycle. The high sensitivity can be attributed to the conductive network established by PANI, providing efficient electron transfer pathways [17,47]. In addition, the hydrogel-based senor possesses excellent long-

term stability, as shown in Fig. 6f. After 300 loading–unloading cycles with a tensile strain of 100 %, the $\Delta R/R_o$ remained almost unchanged, confirming that the sensor did not show significant degradation during long-term cyclic tensile strain. The hydrogel also demonstrated rapid strain responsiveness, with a response time of 223 ms and a recovery time of 191 ms (Fig. 6g). Similarly, the response signals of the PSA/LiCl$_2$/PANI$_{0.30}$ hydrogels exhibited notable distinctions at various pressure levels (1 kPa, 5 kPa, 50 kPa, 100 kPa, and 200 kPa) during five cycles of compression and release, effectively generating precise real-time electrical feedback signals (Fig. 6h). The sensitivity plot encompasses multiple regions (0.0348 kPa^{-1} from 0 to 35 kPa, 0.0268 kPa^{-1} from 35 to 85 kPa, and 0.0202 kPa^{-1} from 85 to 200 kPa) (Fig. S11). Importantly, it is worth noting that the response signals for displacement rates spanning from 50 to 250 mm min^{-1} exhibit virtually identical patterns (Fig. 6i).

The outstanding sensitivity and stable electrical signal output, allow the PSA/LiCl$_2$/PANI$_{0.30}$ hydrogel-based sensor to be suitable for detecting various human motions. As shown in Fig. 7a (and Supporting Movie 3), the composite hydrogels were assembled on human fingers to monitor the finger bending process. The resistance of hydrogels
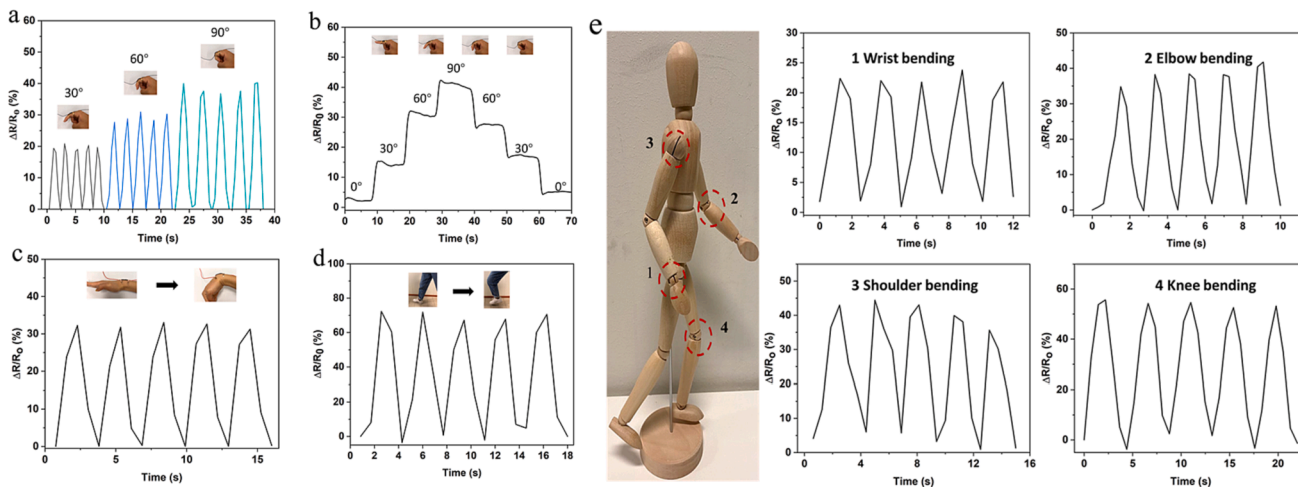
Fig. 7. Relative resistance changes of the sensor (a) during consecutive bending cycle of finger with the index at 30°, 60° and 90°. (b) Gradually bended from 0° to 30°, 60° and 90°. (c) During consecutive bending cycle of wrist and (d) knee. (e) Imitative human joints motions: wrist joint bending, elbow joint bending, shoulder joint bending, and knee joint bending.
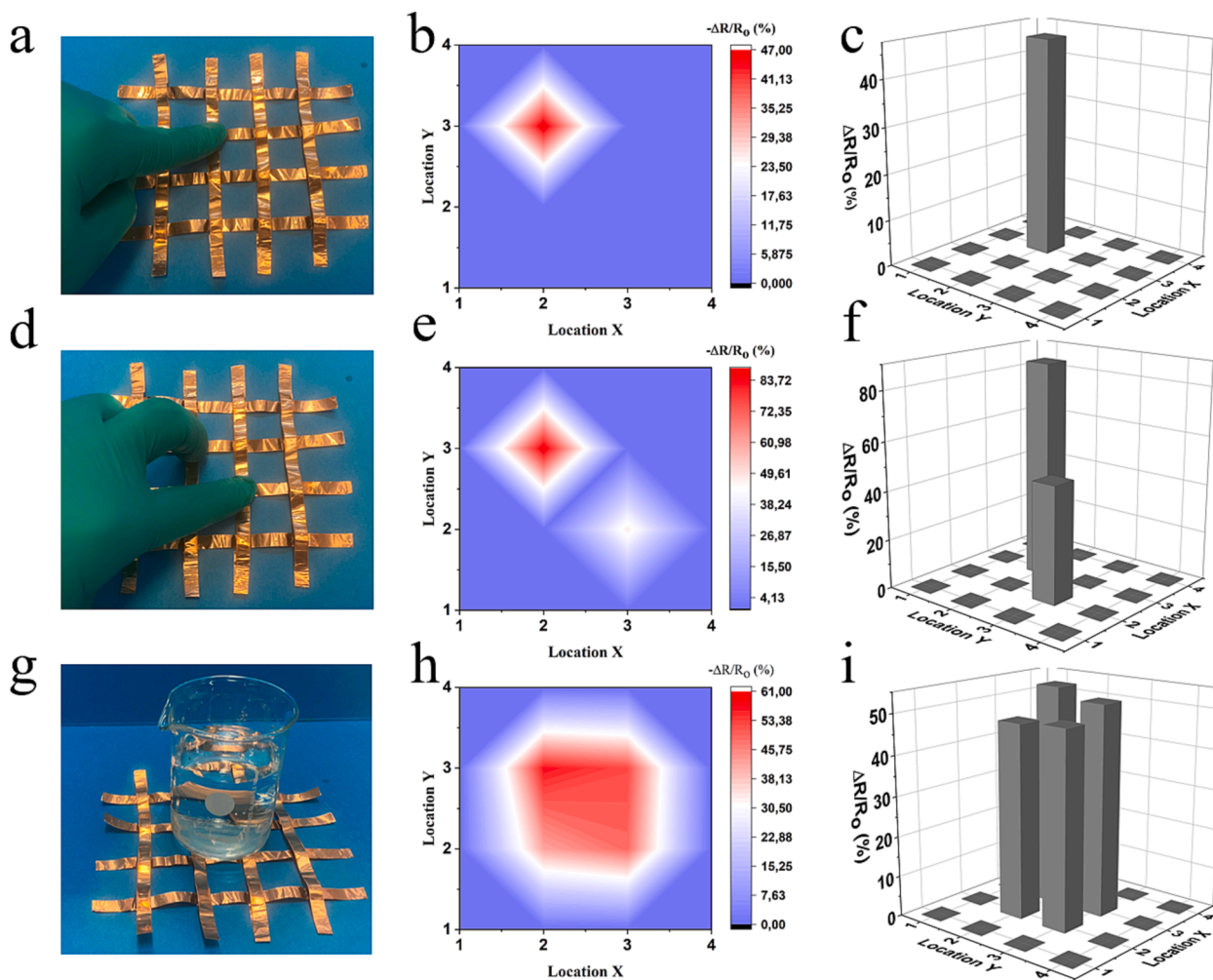
Fig. 8. (a) Photograph capturing the pressure sensor of a single finger touch, along with its corresponding pressure distribution, (b) 2D mapping, and (c) 3D mapping of the sensing response; (d) photograph depicting the pressure sensor with two fingers touch, displaying the pressure distribution, (e) 2D mapping, and (f) 3D mapping of the sensing response; (g) Photograph of a glass beaker with 100 ml of water on pressure sensor, along with the corresponding pressure distribution, (h) 2D mapping, and (i) 3D mapping of the sensing response.

increased when the finger was flexed and returned to the initial value after straightening, with almost the same real-time $\Delta R/R_o$ changes for 5 cycles. The $\Delta R/R_o$ value increased significantly with the gradual increase of the bending angle from $0°$ to $90°$, and the $\Delta R/R_o$ at the same bending angle remained unchanged (Fig. 7b). Therefore, different degrees of motion can be tracked in time and accurately by monitoring changes in relative electrical signals. Similarly, wrist movements can be detected by strain sensors with high stability and repeatability (Fig. 7c). For considerable oscillations in movement, such as during the alternation between bending and straightening of the knee, the ratio of change in resistance to the initial resistance ($\Delta R/R_o$) exhibited a periodic increase and decrease, manifesting the electrical signal's remarkable reproducibility and stability. (Fig. 7d). Considering the anti-freezing performance of the PSA/LiCl/PANI hydrogel, the strain sensors could be also used to monitor physiological motions under subzero temperature. As shown in Fig. 7e, a strain sensor previously kept in the freezer at -18 °C, was immediately mounted on a human model to record $\Delta R/R_o$ during stretching cycles by simulating typical human movements, including wrist, elbow, shoulder and knee (although on a smaller scale). During the bending or relaxation cycle period, the value of $\Delta R/R_o$ increased and recovered periodically, which proved that the hydrogel could still be used to detect physiological activities at low temperature.

Furthermore, the excellent mechanical toughness and sensitivity to external pressure endowed the PSA/LiCl$_2$/PANI$_{0.30}$ hydrogel with the ability to function as a pressure sensor. As a preliminary demonstration, multiple miniature pressure sensors were assembled into a 4×4 array, connected by conductive copper tapes. Pressing the array with a finger produced a pressure signal distribution (Fig. 8a–c), while pressing the array with two fingers (Fig. 8d–f) resulted in a divergent distribution of signals indicative of resistance change at the sensing points. When a glass beaker with 100 ml of water was put on the sensor array, the latter can identify the magnitude and location of the corresponding pressure (Fig. 8g–i). The composite hydrogels exhibited sensitive responsiveness under compression and the differences could be accurately identified from the sensor response signal map. The ability to clearly distinguish between different magnitude and location of pressure, indicates that this hydrogel can also be applied for pressure sensing applications.

4. Conclusions

In summary, we have developed a tough anti-freezing zwitterionic conductive hydrogel with excellent movement and pressure sensing performance. The zwitterionic groups of SBMA present in the chemical structure and the introduced LiCl, provide excellent anti-freezing properties. The hydrogels showed remarkable mechanical properties, especially when a lower SBMA/AA monomers ratio was used, and remained flexible even after being placed at -18 °C for 30 days; moreover, they maintained 68 % of their original mass when kept in open air for two weeks, due to the strong hydration of Li$^+$ ions. The PANI co-network embedded in the hydrogel matrix greatly enhances the mechanical strength and elasticity of the corresponding hydrogels (reaching a fracture tensile strength of 470 kPa, and elongation at break of 600 %). The inclusion of PANI also provides the hydrogel with a higher electrical conductivity, reaching values of 2.23 S m^{-1}, due to the conductive pathway it creates. Concentrations of both LiCl and PANI were optimized for sensing performances. The prepared hydrogels exhibits high electrical sensitivity (GF up to 1.74 at 100–400 % strain), which allows to distinguish various extent of strain. After 300 loading–unloading cycles, the hydrogel still outputs electrical signal reliably. Finally, the hydrogels could be assembled as strain sensors for accurately detecting a variety of human movements, including finger, wrist, and knee flexion. The assembly into an array of pressure sensors allows to clearly distinguish between different magnitudes and locations of applied pressure. Moreover, the conductivity of the prepared hydrogels still keep a value of 1.89 S m^{-1} at -18 °C. Due to the remarkable anti-freezing properties of these PSA/LiCl/PANI hydrogels, strain

sensors can also be used to monitor physiological movements at subzero temperatures. Compared with previously reported results (Table S3), hydrogels in this work present superior electrical properties and high sensitivity, with the ability to operate at low temperature. Further investigation of such and analogous systems should also take into account biocompatibility of the hydrogels with human skin. It may be necessary, for example, to adjust pH values to less acidic ones, due to the presence of carboxylic acid groups.

Nonetheless, we believe that flexible sensors based on anti-freezing zwitterionic hydrogels hold great promise for use in the next generation of multifunctional sensing devices.

CRediT authorship contribution statement

Zeyu Zhang: Investigation, Methodology, Writing – original draft. **Patrizio Raffa:** Conceptualization, Writing – review & editing, Supervision.

Declaration of Competing Interest

The authors declare the following financial interests/personal relationships which may be considered as potential competing interests: Zeyu Zhang reports financial support was provided by China Scholarship Council.

Data availability

Data will be made available on request.

Acknowledgements

Appendix A. Supplementary material

Supplementary data to this article can be found online at https://doi.org/10.1016/j.eurpolymj.2023.112484.

References

[1] Y.J. Ma, Y.C. Zhang, S.S. Cai, Z.Y. Han, X. Liu, F.L. Wang, Y. Cao, Z.H. Wang, H. F. Li, Y.H. Chen, X. Feng, Flexible hybrid electronics for digital healthcare, Adv. Mater. 32 (2020), 1902062, https://doi.org/10.1002/adma.201902062.

[2] M. Khatib, O. Zohar, H. Haick, Self-healing soft sensors: from material design to implementation, Adv. Mater. 33 (2021), 2004190, https://doi.org/10.1002/adma.202004190.

[3] B. Shih, D. Shah, J.X. Li, T.G. Thuruthel, Y.L. Park, F. Iida, Z.A. Bao, R. Kramer-Bottiglio, M.T. Tolley, Electronic skins and machine learning for intelligent soft robots, Sci. Rob. 5 (2020), eaaz9239, https://doi.org/10.1126/scirobotics.aaz9239.

[4] A. Rivadeneyra, A. Marin-Sanchez, B. Wicklein, J.F. Salmeron, E. Castillo, M. Bobinger, A. Salinas-Castillo, Cellulose nanofibers as substrate for flexible and biodegradable moisture sensors, Compos. Sci. Technol. 208 (2021), 108738, https://doi.org/10.1016/j.compscitech.2021.108738.

[5] J. Le Bideau, L. Viau, A. Vioux, Ionogels, ionic liquid based hybrid materials, Chem. Soc. Rev. 40 (2011) 907–925, https://doi.org/10.1039/c0cs00059k.

[6] J.W. Suen, N.K. Elumalai, S. Debnath, N.M. Mubarak, C.I. Lim, M.M. Reddy, The role of interfaces in ionic liquid-based hybrid materials (Ionogels) for sensing and energy applications, Adv. Mater. Interfaces 9 (2022), 2201405, https://doi.org/10.1002/admi.202201405.

[7] Y.P. Yang, H.J. Wang, Y.Y. Hou, S.Q. Nan, Y.Y. Di, Y. Dai, F. Li, J. Zhang, MWCNTs/PDMS composite enabled printed flexible omnidirectional strain sensors for wearable electronics, Compos. Sci. Technol. 226 (2022), 109518, https://doi.org/10.1016/j.compscitech.109518.

[8] T. Cheng, Y.Z. Zhang, S. Wang, Y.L. Chen, S.Y. Gao, F. Wang, W.Y. Lai, W. Huang, Conductive hydrogel-based electrodes and electrolytes for stretchable and self-healable supercapacitors, Adv. Funct. Mater. 31 (2021), 2101303, https://doi.org/10.1002/adfm.202101303.

[9] Z.W. Wang, Y. Cong, J. Fu, Stretchable and tough conductive hydrogels for flexible pressure and strain sensors, J. Mater. Chem. B 8 (2020) 3437–3459, https://doi.org/10.1039/c9tb02570g.

[10] Y. Ohm, C.F. Pan, M.J. Ford, X.N. Huang, J.H. Liao, C. Majidi, An electrically conductive silver-polyacrylamide-alginate hydrogel composite for soft electronics, Nat. Electron. 4 (2021) 313, https://doi.org/10.1038/s41928-021-00571-3.

[11] X. Sun, Z.H. Qin, L. Ye, H.T. Zhang, Q.Y. Yu, X.J. Wu, J.J. Li, F.L. Yao, Carbon nanotubes reinforced hydrogel as flexible strain sensor with high stretchability and mechanically toughness, Chem. Eng. J. 382 (2020) 122832, https://doi.org/10.1016/j.cej.2019.122832.

[12] R.A. Li, T. Fan, G.X. Chen, K.L. Zhang, B. Su, J.F. Tian, M.H. He, Autonomous self-healing, antifreezing, and transparent conductive elastomers, Chem. Mater. 32 (2020) 874–881, https://doi.org/10.1021/acs.chemmater.9b04592.

[13] L.V. Kayser, D.J. Lipomi, Stretchable conductive polymers and composites based on PEDOT and PEDOT:PSS, Adv. Mater. 31 (2019), 1806133, https://doi.org/10.1002/adma.201806133.

[14] K.H. Lee, Y.Z. Zhang, H. Kim, Y.J. Lei, S. Hong, S. Wustoni, A. Hama, S. Inal, H. N. Alshareef, Muscle fatigue sensor based on Ti3C2Tx MXene hydrogel, Small Methods 5 (2021) 2100819, https://doi.org/10.1002/smtd.202100819.

[15] N.K. Guimard, N. Gomez, C.E. Schmidt, Conducting polymers in biomedical engineering, Prog. Polym. Sci. 32 (2007) 876–921, https://doi.org/10.1016/j.progpolymsci.2007.05.012.

[16] D.K. Wang, F.S. Yang, C.P. Wang, F.X. Chu, J.Y. Nan, R.Q. Chen, In-situ polymerization of PANI on hydrogel electrolyte enabling all-in-one supercapacitors mechanically stable at low temperatures, Chem. Eng. J. 455 (2023) 140949, https://doi.org/10.1016/j.cej.2022.140949.

[17] J. Wang, Y.K. Lin, A. Mohamed, Q.M. Ji, H.B. Jia, High strength and flexible aramid nanofiber conductive hydrogels for wearable strain sensors, J. Mater. Chem. C 9 (2021) 575–583, https://doi.org/10.1039/d0tc02983a.

[18] Y. Jiao, Y. Lu, K.Y. Lu, Y.Y. Yue, X.W. Xu, H.N. Xiao, J. Li, J.Q. Han, Highly stretchable and self-healing cellulose nanofiber-mediated conductive hydrogel towards strain sensing application, J. Colloid Interface Sci. 597 (2021) 171–181, https://doi.org/10.1016/j.jcis.2021.04.001.

[19] Z.H. Qin, X. Sun, H.T. Zhang, Q.Y. Yu, X.Y. Wang, S.S. He, F.L. Yao, J.J. Li, A transparent, ultrastretchable and fully recyclable gelatin organohydrogel based electronic sensor with broad operating temperature, J. Mater. Chem. A 8 (2020) 4447–4456, https://doi.org/10.1039/c9ta13196e.

[20] J.W. Wang, H.Y. Wang, B.B. Liu, Z.X. Li, J.Y. Zhang, G.S. Yang, P. Hiralal, S.Y. Jin, H. Zhou, Flexible and anti-freezing zinc-ion batteries using a guar-gum/sodium-alginate/ethylene-glycol hydrogel electrolyte, Energy Stor. Mater. 41 (2021) 599–605, https://doi.org/10.1016/j.ensm.2021.06.034.

[21] D.Q. Bao, Z. Wen, J.H. Shi, L.J. Xie, H.X. Jiang, J.X. Jiang, Y.Q. Yang, W.Q. Liao, X. H. Sun, An anti-freezing hydrogel based stretchable triboelectric nanogenerator for biomechanical energy harvesting at sub-zero temperature, J. Mater. Chem. A 8 (2020) 13787–13794, https://doi.org/10.1039/d0ta03215h.

[22] G.Q. Chen, J.R. Huang, J.F. Gu, S.J. Peng, X.T. Xiang, K. Chen, X.X. Yang, L. H. Guan, X.C. Jiang, L.X. Hou, Highly tough supramolecular double network hydrogel electrolytes for an artificial flexible and low-temperature tolerant sensor, J. Mater. Chem. A 8 (2020) 6776–6784, https://doi.org/10.1039/d0ta00002g.

[23] C.Y. Song, J.K. Wang, S. Li, X.Q. Zou, H.X. Yin, Y.C. Huang, F.L. Dong, P.Y. Li, Y. T. Song, Construction and characterization of highly stretchable ionic conductive hydrogels for flexible sensors with good anti-freezing performance, Eur. Polym. J. 186 (2023) 111827, https://doi.org/10.1016/j.eurpolymj.2023.111827.

[24] X.J. Sui, H.S. Guo, P.G. Chen, Y.N. Zhu, C.Y. Wen, Y.H. Gao, J. Yang, X.Y. Zhang, L. Zhang, Zwitterionic osmolyte-based hydrogels with antifreezing property, high conductivity, and stable flexibility at subzero temperature, Adv. Funct. Mater. 30 (2020), 1907986, https://doi.org/10.1002/adfm.201907986.

[25] Y. Zhang, J.C. Mao, W.K. Jiang, S. Zhang, L. Tong, J.H. Mao, G. Wei, M. Zuo, Y. H. Ni, Lignin sulfonate induced ultrafast polymerization of double network hydrogels with anti-freezing, high strength and conductivity and their sensing applications at extremely cold conditions, Compos. Part B-Eng 217 (2021), 108879, https://doi.org/10.1016/j.compositesb.2021.108879.

[26] L.D. Blackman, P.A. Gunatillake, P. Cass, K.E.S. Locock, An introduction to zwitterionic polymer behavior and applications in solution and at surfaces, Chem. Soc. Rev. 48 (2019) 757–770, https://doi.org/10.1039/c8cs00508g.

[27] X. Peng, H.L. Liu, Q. Yin, J.C. Wu, P.Z. Chen, G.Z. Zhang, G.M. Liu, C.Z. Wu, Y. Xie, A zwitterionic gel electrolyte for efficient solid-state supercapacitors, Nat. Commun. 7 (2016), 11782, https://doi.org/10.1038/ncomms11782.

[28] Q.S. Li, C.Y. Wen, J. Yang, X.C. Zhou, Y.N. Zhu, J. Zheng, G. Cheng, J. Bai, T. Xu, J. Ji, S.Y. Jiang, L. Zhang, P. Zhang, Zwitterionic biomaterials, Chem. Rev. 122 (2022) 17073–17154, https://doi.org/10.1021/acs.chemrev.2c00344.

[29] F.N. Mo, Z. Chen, G.J. Liang, D.H. Wang, Y.W. Zhao, H.F. Li, B.B. Dong, C.Y. Zhi, Zwitterionic sulfobetaine hydrogel electrolyte building separated positive/negative ion migration channels for aqueous Zn-MnO2 batteries with superior rate capabilities, Adv. Energy Mater. 11 (2021), 2100798, https://doi.org/10.1002/aenm.202100798.

[30] X.B. Sun, X.Q. Liu, P. Huang, Z.Y. Wang, Y.F. He, P.F. Song, R.M. Wang, Tri-cationic copolymer hydrogels with adjustable adhesion and antibacterial properties for flexible wearable sensors, J. Mater. Chem. C 11 (2023) 6451–6458, https://doi.org/10.1039/d3tc00746d.

[31] Y. Zhang, H. Liu, P. Wang, Y.Y. Yu, M. Zhou, B. Xu, L. Cui, Q. Wang, Stretchable, transparent, self-adhesive, anti-freezing and ionic conductive nanocomposite hydrogels for flexible strain sensors, Eur. Polym. J. 186 (2023) 111824, https://doi.org/10.1016/j.eurpolymj.2023.111824.

[32] J.B. Yang, Z. Xu, J.J. Wang, L.G. Gai, X.X. Ji, H.H. Jiang, L.B. Liu, Antifreezing zwitterionic hydrogel electrolyte with high conductivity of 12.6 mS cm^{-1} at $-40°C$

[33] C. Tiyapiboonchaiya, J.M. Pringle, J.Z. Sun, N. Byrne, P.C. Howlett, D. R. Macfarlane, M. Forsyth, The zwitterion effect in high-conductivity polyelectrolyte materials, Nat. Mater. 3 (2004) 29–32, https://doi.org/10.1038/nmat1044.

[34] S.Y. Zheng, S.H. Mao, J.F. Yuan, S.B. Wang, X.M. He, X.N. Zhang, C. Du, D. Zhang, Z.L. Wu, J.T. Yang, Molecularly engineered zwitterionic hydrogels with high toughness and self-healing capacity for soft electronics applications, Chem. Mater. 33 (2021) 8418–8429, https://doi.org/10.1021/acs.chemmater.1c02781.

[35] D.Y. Dong, C. Tsao, H.C. Hung, F.L. Yao, C.J. Tang, L.Q. Niu, J.R. Ma, J. MacArthur, A. Sinclair, K. Wu, P. Jain, M.R. Hansen, D. Ly, S.G.H. Tang, T. M. Luu, P. Jain, S.Y. Jiang, High-strength and fibrous capsule-resistant zwitterionic elastomers, Sci. Adv. 7 (2021), eabc5442, https://doi.org/10.1126/sciadv.abc5442.

[36] T.J. Xu, L. Zhang, B.W. Song, X. Bai, Z.X. Huang, X.D. Bu, T.T. Chen, H. Fu, P. P. Guo, High-strain sensitive zwitterionic hydrogels with swelling-resistant and controllable rehydration for sustainable wearable sensor, J. Colloid Interface Sci. 620 (2022) 14–22, https://doi.org/10.1016/j.jcis.2022.03.125.

[37] X.J. Sui, H.S. Guo, C.C. Cai, Q.S. Li, C.Y. Wen, X.Y. Zhang, X.D. Wang, J. Yang, L. Zhang, Ionic conductive hydrogels with long-lasting antifreezing, water retention and self-regeneration abilities, Chem. Eng. J. 419 (2021) 129478, https://doi.org/10.1016/j.cej.2021.129478.

[38] J. Zhao, G.C. Ji, Y. Li, R.F. Hu, J.P. Zheng, Preparation of a self-healing polyaniline-based gel and its application as a healable all-in-one capacitor, Chem. Eng. J. 420 (2021), 129790, https://doi.org/10.1016/j.cej.2021.129790.

[39] Q.Z. Yu, Crystal structure and property of proton acid and polypeptide co-doped polyaniline, J. Phys. Chem. C 120 (2016) 27628–27634, https://doi.org/10.1021/acs.jpcc.6b07969.

[40] Z.X. Zhou, Z.R. He, S.W. Yin, X.Y. Xie, W.Z. Yuan, Adhesive, stretchable and antibacterial hydrogel with external/self-power for flexible sensitive sensor used as human motion detection, Compos. Part B-Eng 220 (2021), 108984, https://doi.org/10.1016/j.compositesb.2021.108984.

[41] Z.Y. Lei, P.Y. Wu, A supramolecular biomimetic skin combining a wide spectrum of mechanical properties and multiple sensory capabilities, Nat. Commun. 9 (2018), 1134, https://doi.org/10.1038/s41467-018-03456-w.

[42] P. Kolle, R. Dronskowski, Hydrogen bonding in the crystal structures of the ionic liquid compounds butyldimethylimidazolium hydrogen sulfate, chloride, and chloroferrate(II, III), Inorg. Chem. 43 (2004) 2803–2809, https://doi.org/10.1021/ic035237l.

[43] J. Cong, Z.W. Fan, S.S. Pan, J. Tian, W.Z. Lian, S. Li, S.J. Wang, D.C. Zheng, C. G. Miao, W.P. Ding, T.L. Sun, T.Z. Luo, Polyacrylamide/chitosan-based conductive double network hydrogels with outstanding electrical and mechanical performance at low temperatures, ACS Appl. Mater. Interfaces 13 (2021) 34942–34953, https://doi.org/10.1021/acsami.1c08421.

[44] G.H. Su, S.Y. Yin, Y.H. Guo, F. Zhao, Q.Q. Guo, X.X. Zhang, T. Zhou, G.H. Yu, Balancing the mechanical, electronic, and self-healing properties in conductive self-healing hydrogel for wearable sensor applications, Mater. Horiz. 8 (2021) 1795–1804, https://doi.org/10.1039/d1mh00085c.

[45] Z.Y. Zhang, Z. Zheng, Y.L. Zhao, J.H. Hu, H.T. Wang, Highly stretchable porous composite hydrogels with stable conductivity for strain sensing, Compos. Sci. Technol. 213 (2021), 108968, https://doi.org/10.1016/j.compscitech.2021.108968.

[46] Z. Chen, J. Liu, Y.J. Chen, X. Zheng, H.Z. Liu, H. Li, Multiple-stimuli-responsive and cellulose conductive ionic hydrogel for smart wearable devices and thermal actuators, ACS Appl. Mater. Interfaces 13 (2021) 1353–1366, https://doi.org/10.1021/acsami.0c16719.

[47] Z.W. Wang, J. Chen, Y. Gong, H. Zhang, T. Xu, L. Nie, J. Fu, Ultrastretchable strain sensors and arrays with high sensitivity and linearity based on super tough conductive hydrogels, Chem. Mater. 30 (2018) 8062–8069, https://doi.org/10.1021/acs.chemmater.8b03999.

[48] L.G. Xu, Z.K. Huang, Z.S. Deng, Z.K. Du, T.L. Sun, Z.H. Guo, K. Yue, A. Transparent, Highly stretchable, solvent-resistant, recyclable multifunctional ionogel with underwater self-healing and adhesion for reliable strain sensors, Adv. Mater. 33 (2021), 2105306, https://doi.org/10.1002/adma.202105306.

[49] J.Y. Ren, Y.H. Liu, Z.Q. Wang, S.Q. Chen, Y.F. Ma, H. Wei, S.Y. Lu, An anti-swellable hydrogel strain sensor for underwater motion detection, Adv. Funct. Mater. 32 (2022), 2107404, https://doi.org/10.1002/adfm.202107404.

[50] Y. Ma, Y. Gao, L. Liu, X.Y. Ren, G.H. Gao, Skin-contactable and antifreezing strain sensors based on bilayer hydrogels, Chem. Mater. 32 (2020) 8938–8946, https://doi.org/10.1021/acs.chemmater.0c02919.

[51] Y.Q. Yang, L. Guan, X.Y. Li, Z.J. Gao, X.Y. Ren, G.H. Gao, Conductive organohydrogels with ultrastretchability, antifreezing, self-healing, and adhesive properties for motion detection and signal transmission, ACS Appl. Mater. Interfaces 11 (2019) 3428–3437, https://doi.org/10.1021/acsami.8b17440.

[52] S.W. Huang, L. Hou, T.Y. Li, Y.C. Jiao, P.Y. Wu, Antifreezing hydrogel electrolyte with ternary hydrogen bonding for high-performance zinc-ion batteries, Adv. Mater. 34 (2022), 2110140, https://doi.org/10.1002/adma.202110140.

[53] H.G. Wei, D.S. Kong, T. Li, Q.Z. Xue, S.Y. Wang, D.P. Cui, Y.D. Huang, L. Wang, S. M. Hu, T. Wan, G. Yang, Solution-processable conductive composite hydrogels with multiple synergetic networks toward wearable pressure/strain sensors, ACS Sens. 6 (2021) 2938–2951, https://doi.org/10.1021/acssensors.1c00699.